

Optical properties of low molecular weight and colloidal organic matter: Application of the ultrafiltration permeation model to DOM absorption and fluorescence

Claude Belzile^{*}, Laodong Guo¹

International Arctic Research Center, University of Alaska Fairbanks, Fairbanks, AK 99775, United States

Accepted 30 August 2005

Available online 15 November 2005

Abstract

Cross-flow ultrafiltration (CFF) is often used to obtain separation and concentration of colloids from bulk natural water samples. Application of the ultrafiltration permeation model allows the quantitative determination of the low molecular weight material (LMW, <1 kDa) and colloids in bulk dissolved organic matter (DOM) from measurements of time series permeate samples obtained from CFF. Detailed analysis of a Yukon River water sample shows that DOM absorption coefficient and fluorescence follow the permeation model and that the complex spectral optical properties of LMW DOM can be reconstructed from CFF data. A combination of measured and modeled data indicates that the LMW contribution to bulk DOM optical properties obtained from CFF can be grossly underestimated by the use of a low concentration factor (CF, the ratio of initial sample volume to retentate volume). Even at a relatively high CF of 19, optical properties of LMW DOM calculated from measurements of the retentate or integrated permeate would underestimate true values by 5–36%. In the Yukon River sample, LMW dissolved organic carbon represented 26% of the bulk concentration, but only 3–14% of the colored DOM was in the LMW fraction while 31–33% of bulk DOM fluorescence was due to LMW DOM. The contrasting optical properties of LMW and colloidal DOM support the concept that analysis of bulk DOM absorption and fluorescence properties reveals information about DOM molecular weight.

© 2005 Elsevier B.V. All rights reserved.

Keywords: Colored dissolved organic matter; Dissolved organic carbon; Absorption coefficient; Fluorescence; Colloids; Ultrafiltration; Biogeochemistry; Yukon River; Alaska

1. Introduction

The size distribution of dissolved organic matter (DOM) largely influences its fate and biogeochemical cycling in aquatic environments. The size-reactivity continuum model linking the physical size of organic matter to its diagenetic state suggests a decrease in size with increasing diagenesis and chemical alteration (Amon and Benner, 1996). Decrease in molecular weight with increasing diagenesis is the result of a complex suite of microbial degradation (e.g., Hama et al., 2004) and photochemical alterations (e.g., Moran

^{*} Corresponding author. Now at: Institut des Sciences de la Mer de Rimouski, Université du Québec à Rimouski, 310 Allée des Ursulines, Rimouski, Québec, Canada G5L 3A1. Tel.: +1 418 723 1986; fax: +1 418 724 1842.

E-mail addresses: claude_belzile@uqar.qc.ca (C. Belzile), laodong.guo@usm.edu (L. Guo).

¹ Current address: Department of Marine Science, University of Southern Mississippi, Stennis Space Center, MS 39529, United States.

and Zepp, 1997) of the organic matter pool. Knowledge of DOM partitioning between different size- or molecular weight classes therefore provides insights into understanding its biogeochemistry. However, obtaining quantitative separation of DOM based on size or molecular weight has been difficult and plagued with numerous methodological problems and limitations (Buesseler et al., 1996; Guo et al., 2000; Vaillancourt and Balch, 2000; Scully et al., 2004). Among the most frequently used separation techniques are resin adsorption chromatography (using synthetic resins such as XAD-8 and XAD-4), reverse osmosis, cross-flow ultrafiltration (CFF), size exclusion chromatography (SEC), and flow field-flow fractionation (FFFF). CFF has proven to be one of the most useful techniques to obtain separation and concentration of colloids from bulk natural water samples. The CFF technique is a pressure-driven process that separates macromolecules based on the ultrafiltration membrane pore dimensions. Unlike conventional dead-point filtration, membrane clogging during CFF is greatly reduced by the cross flow of fluid. The molecular weight cut-off value of a given CFF membrane is usually defined as the smallest molecular mass species for which the membrane exhibits a 90% rejection. Unlike other separation techniques where only absorbing DOM is detected (for example, SEC and FFFF in most instance), a wide variety of biogeochemical variables can be measured on the low molecular weight (LMW) and high molecular weight (HMW) fractions obtained from CFF.

According to the ultrafiltration permeation model (see Logan and Jiang, 1990 for details) the concentration of a given compound in the permeate of a 1 kDa ultrafiltration membrane, C_p , follows:

$$\ln C_p = (1 - PC)\ln(CF) + \ln(PC C_{LMW}) \quad (1)$$

where PC is the permeation coefficient for that compound, CF is the concentration factor (the ratio of initial volume to retentate volume) and C_{LMW} is the LMW concentration of that compound in the original bulk sample. A linear relationship between $\ln C_p$ and $\ln CF$ indicates a constant permeation behavior. Previous studies have shown that many organic and inorganic compounds indeed obey the permeation model (e.g., Logan and Jiang, 1990; Guo and Santschi, 1996; Guo et al., 2000, 2001). From Eq. (1), it follows that the PC and C_{LMW} values of a given chemical species can be calculated from the slope and intercept of the linear relationship between $\ln C_p$ and $\ln CF$:

$$PC = 1 - \text{slope} \quad (2)$$

and

$$C_{LMW} = \exp(\text{intercept})/PC \quad (3)$$

Determination of the time series permeate concentrations therefore allows the calculation of the concentration of LMW molecules in the original sample and, by difference, the colloid concentration.

It remains debated whether a better separation of colloids and LMW DOM by CFF is achieved using a low or a high CF (Wells, 2002). Despite the demonstration by Guo and Santschi (1996) and Guo et al. (2000) that a high CF (i.e., $CF > 40$) is necessary to decrease the relative contribution of LMW DOM to the retentate (a phenomenon well described by the ultrafiltration permeation model), many authors are still using a $CF \ll 10$. The common misperception that CFF is similar to conventional filtration explains much of the misuses and wrong interpretations of the LMW and colloids behavior during CFF. Since a fraction of the water molecules ($MW = 0.018$ kDa) is kept in the retentate during CFF, it is not surprising that some LMW material is also retained. Increasing CF decreases the fraction of water molecules retained and simultaneously the concentration of LMW material in the retentate. The retention of LMW material implies that measurements made on the retentate overestimate the true colloid concentration, especially at low CF. On the other hand, measurements made on an integrated permeate sample underestimate true LMW concentration. Measurements of permeate time series samples and application of the permeation model, although it requires much more work, is the only approach allowing true LMW and colloidal fractions to be determined. Nevertheless, it is still unknown if the spectral optical properties of DOM follow the permeation model (the optical properties of DOM reflecting the complex mixture of the optical properties of individual components).

The optical properties of DOM contain information regarding the chemical composition, origin and diagenesis stage of the material. The absorption and fluorescence of DOM are the optical properties that received the most attention, although DOM scattering also has useful application for the study of colloids (dynamic laser scattering; Chin et al., 1998). Many studies have shown relationships between the optical properties and molecular weight of DOM. For instance, the ratio of dissolved matter absorption, $a_g(\lambda)$, to DOC concentration (or DOC-specific $a_g(\lambda)$) increases with the average molecular weight of DOM (Traina et al., 1990; Chin et al., 1994; Yacobi et al., 2003). More than 25 years ago, the ratio of fluorescence to absorption (or fluorescence quantum yield) was proposed as a molecular-weight

tracer of DOM (Stewart and Wetzel, 1980). These authors found that the apparent fluorescence quantum yield of LMW DOM isolated using dialysis and gel permeation chromatography was much higher than that of the HMW DOM. However, questions remain regarding the results of these early investigations because of artifacts caused by the isolation techniques, errors in the determination of DOC concentration, or improper treatment of the optical signal. One important issue is that the fluorescence intensity and fluorescence spectral shape are affected by the absorption of the excitation light and emitted photons within the cuvette, the so-called inner-filter effect (McKnight et al., 2001; Ohno, 2002). Differences attributed to molecular weight can be caused by the very different absorption properties of the LMW and colloidal fractions, with the concentrated colloidal fraction having a much stronger inner-filter related artifact.

The objective of our study is to characterize the absorption and fluorescence properties of LMW and colloidal DOM in order to use the bulk optical properties as indices of DOM composition. Here we show that the spectral optical properties of DOM from the Yukon River behave as predicted by the permeation model. Analysis of permeate time series samples therefore allows the estimation of the optical properties of LMW DOM and colloids in the original water sample. We show that LMW DOM and colloids have contrasting optical properties that can be used for DOM characterization. In addition, analysis of the optical properties provided information regarding the CFF performance.

2. Methods

2.1. Sampling

A Yukon River water sample was collected on 10 November 2004 at Pilot Station, Alaska (Lat 61.94°N Lon 162.87°W), about 100 km from the river discharge into the Bering Sea. At the time of sampling, the river was covered by newly formed, thin ice (~10–20 cm). A surface water sample was collected from a hole made in the ice about 4 m from the shore (water depth >2 m). Water pH was 7.5 and specific conductivity was 226 $\mu\text{S cm}^{-1}$. The 20 l water sample was filtered immediately through a prerinced 0.45 μm polycarbonate Osmonics cartridge, and the filtrate was stored in the dark at 4 °C until ultrafiltration (20 days later). The DOM absorption and fluorescence properties measured on the fresh sample were within 3% of the values measured when the ultrafiltration was performed, suggesting minimal storage effects.

2.2. Ultrafiltration

A spiral-wound 1 kDa Amicon S10Y1 ultrafiltration cartridge with regenerated cellulose as the membrane material was used for the CFF of the water sample. A Teflon diaphragm pump head was equipped with Teflon fittings and tubing to decrease sorptive losses and any possible contamination from the apparatus. Calibration of this 1 kDa ultrafiltration membrane using standard macromolecules with known molecular weights showed a retention of 84% for 1.3 kDa vitamin B12 (Sigma) and 99% for 4.4 kDa FITC-tagged dextran (Sigma). These calibration results are consistent with the molecular weight cut-off provided by the manufacturer, showing the membrane integrity. The ultrafiltration cartridge and tubing were thoroughly cleaned before each experiment with 1% Micro detergent and 0.05 M NaOH. Each chemical was recycled within the ultrafiltration device for 20 min and soaked for another 20 min. Between each cleaning solution, 20 l of ultrapure water (with a DOC concentration <8 μM) was flushed through the ultrafiltration system. After chemical cleaning, another 40 l of ultrapure water was ultrafiltered under normal operating conditions (except that the retentate line was not returned to the sample reservoir). In order to avoid computation difficulties for the mass balance determination, the clean membrane was not preconditioned with the sample. 12 l of prefiltered water was ultrafiltered at a backpressure of 2.7 atmospheres (40 psi) resulting in a constant permeate flow rate of 89 ml min^{-1} . Discrete samples from the permeate line were collected at eight different concentration factors, ranging from 1.05 to 19.11, to generate time series data points to be fitted to the permeation model (Table 1). Except for these small-volume discrete samples (40 ml each), all permeate was pooled into a so-called 'integrated permeate'. The ultrafiltration was stopped when the retentate volume was reduced to 625 ml (CF=19.1). The deadvolume of the cartridge was recovered by three consecutive washes, each consisting of 200 ml ultrapure water. Since no pressure was applied during these washes and no chemical cleaning agent was used, only material physically retained by membrane or sorbed unto the membrane was recovered during this process. Nevertheless, the washes were not added to the retentate (as usually done) in order to avoid possible concentration-related effects on the optical properties; instead, the three washes were analyzed individually to monitor the recovery during each wash and to gain insights into the optical properties of recovered DOM.

Table 1

Concentrations and optical properties in the bulk sample, permeate time series samples (denoted P1 to P8), integrated permeate (Integ. P), retentate and 3 consecutive washes, and mass balance calculation for each parameter

	Permeate volume (l)	CF	$a_g(370)$ (m^{-1})	FL(450) (RU)	SF(250–650) (RU)	DOC (μM)	TDN (μM)
Bulk sample			10.04	7.08	0.384	453	22.1
P1	0.54	1.05	0.25	0.83	0.048	55	15.0
P2	3.08	1.35	0.32	1.00	0.057	74	13.1
P3	6.12	2.05	0.44	1.39	0.075	89	12.9
P4	8.16	3.16	0.60	1.84	0.098	97	13.7
P5	9.20	4.35	0.76	2.28	0.122	118	14.8
P6	10.24	7.01	1.04	3.04	0.159	157	15.9
P7	10.78	10.25	1.32	3.74	0.198	195	16.6
P8	11.32	19.11	1.81	5.02	0.257	266	18.0
Integ. P	11.32	19.11	0.54	1.64	0.088	96	14.0
Retentate (0.625 L)			109.75	62.57	3.371	4762	118.6
Wash 1 (0.200 L)			125.08	63.15	3.612	4749	117.1
Wash 2 (0.200 L)			65.59	33.44	1.967	2476	70.0
Wash 3 (0.200 L)			20.22	9.34	0.636	789	36.4
Recovery P+R (%)			62	68	68	75	88
Recovery P+R+wash 1 (%)			83	83	83	93	97
Recovery P+R+wash 1–2 (%)			94	91	92	102	102
Recovery P+R+wash 1–3 (%)			97	93	95	105	105

The mass-balance calculations are made considering only the permeate and retentate (recovery P+R), and when the three consecutive washes are also included (recovery P+R+wash).

2.3. DOC and TDN determination

Concentration of DOC and total dissolved nitrogen (TDN, the sum of inorganic and organic N) were measured the day following ultrafiltration on a high-temperature combustion TOC analyzer (TOC-V, Shimadzu) equipped with a total nitrogen measuring unit (TNM-1, Shimadzu). Each sample was injected 3–5 times, and the mean values are reported. An instrument blank of 12 μM C and 1.4 μM N was subtracted from the measured values based on measured concentrations for MilliQ water. The coefficient of variation (CV) of the replicated injections was better than 2%, and measurements of standards containing 416.7 μM C and 357.1 μM N inserted between samples ($N=3$) gave 412.5 ± 3.3 μM for DOC and 349.3 ± 2.1 μM for TDN. Previous studies conducted at our sampling site in the Yukon River suggest that in late fall ~30% of TDN is represented by inorganic forms (Brabets, 2003).

2.4. DOM absorption coefficient and fluorescence

Absorption and fluorescence measurements were made within 4 h of ultrafiltration. The absorption coefficient of dissolved matter, $a_g(\lambda)$, was measured spectrophotometrically in acid-cleaned quartz cuvettes with an Agilent 8453 UV–visible spectrophotometer at 2-nm resolution over the wavelength range 200–850 nm. The measurements were baseline-corrected using MilliQ water from a Millipore Gradient A10 system

(resistivity 18.2 $m\Omega \cdot cm$; total organic carbon=8–10 ppb), running a new blank every 5 samples. The spectra were further corrected for any residual scattering by subtracting the average value measured over the range 790–800 nm. Most samples were measured using a 5-cm cuvette although a 1-cm cuvette was used for the concentrated samples (i.e., retentate and three washes) in order to avoid saturation of the spectrophotometer signal. A non-linear regression of $a_g(\lambda)$ over the range 300–700 nm was made using an exponential model of the form:

$$a_g(\lambda) = a_g(\lambda_o) \exp(-S_g(\lambda - \lambda_o)) \quad (4)$$

where $a_g(\lambda_o)$ is the magnitude of the absorption at reference wavelength λ_o , and S_g is the slope parameter describing the wavelength dependence (see review by Twardowski et al., 2004). A reference wavelength of 370 nm was selected because it is used in a commercially available in situ DOM fluorometer and it is the excitation wavelength used for humic substance fluorescence determination (see below).

DOM fluorescence emission spectra (FL) and synchronous fluorescence spectra (SF) were measured using a Fluoromax-3 Jobin–Yvon spectrofluorometer. Before the measurements, the four most concentrated samples were diluted 1:10 in MilliQ water in order to reduce the absorption of the excitation and emission energy within the samples (the inner-filter effect).

The fluorescence emission over the range 400–700 nm was measured using an excitation wavelength of

370 nm with a 5 nm bandpass for both the emission and excitation (McKnight et al., 2001). The raw FL spectra were corrected for the inner-filter effect according to the procedure outlined in McKnight et al. (2001) but adapted so that $a_g(\lambda)$ can be used instead of absorbance:

$$\text{Corrected FL}(\lambda) = \text{raw FL}(\lambda) / [\exp(-a_g(\lambda_{\text{ex}}) \times 0.005) \times \exp(-a_g(\lambda_{\text{em}}) \times 0.005)] \quad (5)$$

where $a_g(\lambda_{\text{ex}})$ and $a_g(\lambda_{\text{em}})$ are the absorption coefficients at the excitation and emission wavelengths, respectively, and 0.005 is half the pathlength (in m) of the 1-cm cuvette. The MilliQ blank was then subtracted from the corrected spectra. Corrected-fluorescence at 450 nm was expressed relative to the Raman peak height of the MilliQ reference (FL(450), Raman Units). This combination of excitation–emission wavelengths provides an estimation of humic substances concentration (McKnight et al., 2001; Stedmon et al., 2003). The McKnight's aromaticity index (FL(450)/FL(500); McKnight et al., 2001) was also calculated from the FL spectra.

Synchronous fluorescence spectra were measured according to Belzile et al. (2002). Inner-filter-corrected and blank-corrected spectra were integrated over the range 250–650 nm and expressed relative to the MilliQ Raman peak height for excitation at 370 nm (SF(250–650), Raman Units). The integrated SF provides a combined index of the humic substances and protein-like and/or polyphenol fluorescence (Stedmon et al., 2003; Scully et al., 2004) and is therefore representative of most of the fluorescing DOM.

3. Results

3.1. DOM permeation

The CF of 19.1 increased the concentrations in the retentate by a factor of 6–11, depending on the property considered (Table 1; for simplicity, the optical properties are hereafter treated as “concentrations”). When only the permeate and retentate were considered, the recoveries were low for most parameters (62–75%, but 88% for TDN; Table 1). However, including the 3 washes allowed nearly total recoveries (93–105%, Table 1). The concentrations in the first wash were similar to that in the final retentate, suggesting that this wash simply displaced the dead volume of the cartridge. Concentrations in the second and third washes were still significant, and these washes likely recovered material weakly associated with the cellulose ultrafiltration membrane. Extrapolating the measured

concentrations in the washes by assuming a linear decrease with each successive wash suggests that the concentrations would have been negligible in the fourth wash. The recoveries of close to 100% suggest that DOM adsorption to the membrane, if any, was easily reversible.

During the time series measurements of permeate concentrations, $a_g(370)$, FL(450) and SF(250–650) showed a constant permeation behavior as indicated by the linear relationships with $r^2 > 0.99$ between $\ln C_p$ and $\ln CF$ (Fig. 1C and Table 2). These three parameters had similar slopes with values of 0.60–0.69. DOC and TDN concentrations in the permeate time series also had a significant linear relationship between $\ln C_p$ and $\ln CF$ but deviated slightly at low CF (Fig. 1A and C, Table 2). The slope for DOC was slightly lower (0.52) than that of the absorption and fluorescence properties, and TDN had a slope of only 0.10 (Table 2).

From the slope and intercept of the \ln – \ln plots, the concentration of LMW material in the original sample, C_{LMW} , can be calculated using Eq. (2) and Eq. (3). Only 8.3% of $a_g(370)$ was associated with LMW DOM, while 31–33% of the fluorescing DOM and 26% of DOC was in the LMW fraction (Table 2). Most of the TDN was in the LMW fraction (i.e., 65%), likely reflecting a relatively high contribution of inorganic forms to TDN, or a smaller average molecular weight for DON.

The mathematical integration of the concentrations measured for the discrete samples collected during the permeate time series agreed with the integrated permeate values within 2% for all parameters (not shown), indicating the consistency and accuracy of the individual measurements of permeate concentrations.

3.2. Spectral and DOC-specific optical properties

The DOC-specific SF of the integrated permeate was markedly different from that of the retentate, bulk sample and washes, with a much higher relative contribution by the protein-like fluorescence peak centered near 300 nm (Fig. 2A). The retentate DOC-specific SF was similar in shape to that of the bulk sample, consistent with the large contribution of colloids to total SF (69%, Table 2). The magnitude of the permeate SF spectra not normalized by the DOC concentration increased monotonically with CF. The DOC-specific SF of the permeate time series samples showed only small variation in shape (Fig. 2B), indicating that no significant colloid breakthrough occurred even at a relatively high CF.

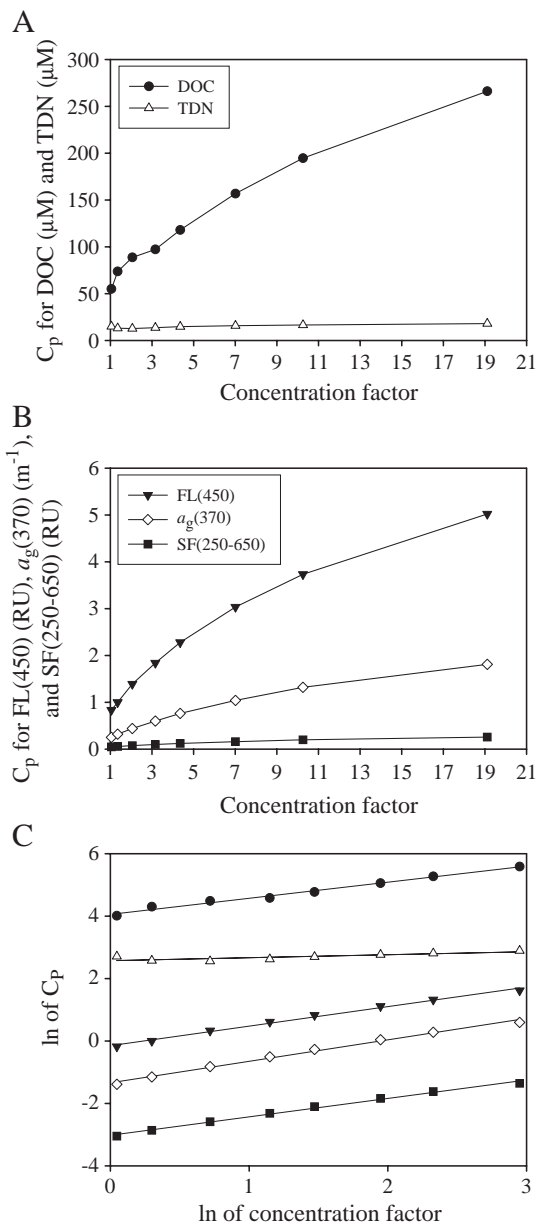


Fig. 1. Time series of the concentrations measured in the permeate (C_p) as a function of the concentration factor (CF); dissolved organic carbon (DOC, μM), total dissolved nitrogen (TDN, μM), fluorescence carbon measured at 450 nm for excitation at 370 nm (FL(450), Raman units), absorption coefficient at 370 nm ($a_g(370)$, m^{-1}), and integrated synchronous fluorescence (SF(250–650), Raman units). (A) and (B) linear scale; (C) $\ln C_p$ vs. $\ln CF$.

The McKnight's aromaticity index (McKnight et al., 2001) calculated from the FL spectra obtained with an excitation at 370 nm also showed marked differences between permeate and retentate fractions (Fig. 3A). The bulk sample, retentate and washes all had indices typical for high aromaticity DOM. The index values of

the permeate point to a very low aromaticity for the LMW DOM, with aromaticity comparable to that of microbially-derived DOM (McKnight et al., 2001). The similarity between the indices of the washes and retentate strongly suggests that the material recovered by the washes indeed belonged to the colloidal fraction. Although the permeate time series data show a decrease in aromaticity index with increasing CF (an increase in aromaticity), the values remained much higher than that of the retentate (1.68–1.82 for the permeate samples compared to 1.46 for the retentate and 1.51 for the bulk sample). The variations of the fluorescence quantum yield between the different fractions (Fig. 3B) showed a pattern strikingly similar to the variations of the McKnight index. The permeate fractions had a quantum yield nearly 3 times higher than any other fraction.

The DOC-specific absorption coefficient is also viewed as an index of aromaticity, with high values associated with DOM of high aromaticity (Traina et al., 1990; Chin et al., 1994). Values of the DOC-specific $a_g(370)$ were at least three times lower in the permeate than in the retentate and bulk sample, consistent with a low aromaticity for the LMW fraction (Fig. 4). In other words, the LMW DOM was much less colored per unit DOC ($0.007 \text{ m}^{-1} \mu\text{M}^{-1}$) than the bulk sample and colloids which had values of 0.022 and $0.028 \text{ m}^{-1} \mu\text{M}^{-1}$, respectively (as calculated from C_{LMW} presented at Table 2). There was a strong inverse correlation between the McKnight index and DOC-specific $a_g(370)$ (Fig. 4, insert); such a strong correlation is remarkable considering that the index computation involves the independently determined fluorescence spectra, absorption coefficients and DOC concentrations.

The slope of $a_g(\lambda)$, S_g , also gives information regarding DOM composition. It is generally accepted that a high S_g value in the UV–visible region is indicative of microbially-derived or highly degraded DOM, while a low slope is more typical of terrestri-

Table 2

Intercept and slope of the linear relationship between $\ln C_p$ and $\ln CF$, regression coefficient and probability, LMW concentration (C_{LMW}) calculated using Eq. (2) and Eq. (3), and percent contribution of LMW DOM to bulk concentration (%LMW)

	Intercept	Slope	r^2	P	C_{LMW}	%LMW
$a_g(370)$	-1.341	0.688	0.993	<0.001	0.839 m^{-1}	8.3
FL(450)	-0.149	0.630	0.993	<0.001	2.329 RU	32.9
SF(250–650)	-3.012	0.600	0.995	<0.001	0.119 RU	31.0
DOC	4.054	0.515	0.988	<0.001	119 μM	26.2
TDN	2.572	0.095	0.671	0.013	14.5 μM	65.4

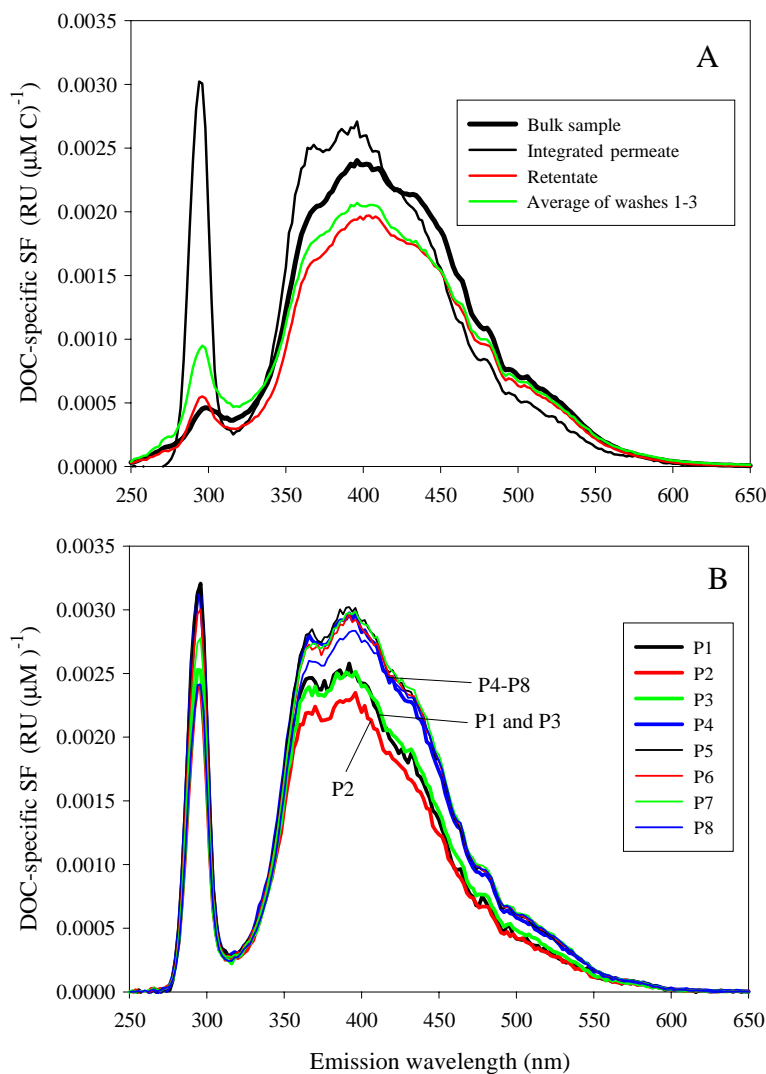


Fig. 2. Synchronous fluorescence spectra normalized to DOC concentration. (A) Bulk sample, integrated permeate, retentate and average of the 3 washes; (B) time series of permeate.

ally-derived DOM or less diagenetically altered material (see reviews by Markager and Vincent, 2000; Twardowski et al., 2004). In agreement with this view, the bulk sample and retentate had a slope of 0.016 nm^{-1} while the LMW DOM had S_g values varying $0.020\text{--}0.021 \text{ nm}^{-1}$ (Fig. 5). Although departures from the exponential fit were observed over the wavelength range 300–700 nm, S_g values determined over the narrower range 350–550 nm (where the data fitted the exponential model almost perfectly) differed by only 1–8% from those measured over the full 300–700 nm range, with the two estimates strongly correlated ($r=0.993$). The S_g values were positively correlated to the McKnight index of aromaticity ($S_g=0.018x-0.012$, $r=0.912$).

3.3. Reconstructed spectral optical properties of LMW DOM

Although the permeation model allows relatively simple estimation of the LMW concentration from permeate time series data, its application to spectral data is more fastidious, as the permeation model must be applied to a large number of data obtained at discrete wavelengths in order to reconstruct the full LMW spectrum. For $a_g(\lambda)$, one simple way to recover the spectrum of LMW DOM is to apply the permeation model to a reference wavelength and then use the slope of the integrated permeate or the average slope of individual permeate measurements (in the present study, the permeate S_g varied only $0.0203\text{--}0.0210 \text{ nm}^{-1}$) together

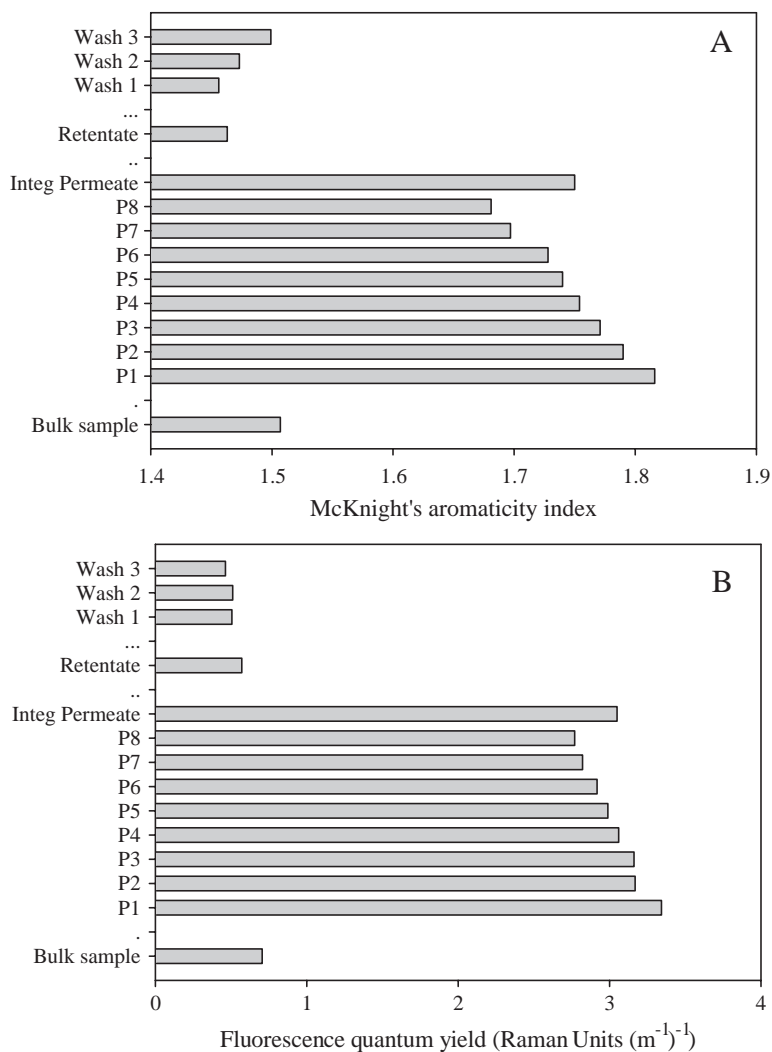


Fig. 3. (A) McKnight's aromaticity index; and (B) fluorescence quantum yield for each fraction. The quantum yield was calculated as the fluorescence emitted at 450 nm for excitation at 370 nm divided by $a_g(370)$. Note that DOM aromaticity decreases with increasing values of the McKnight's aromaticity index.

with Eq. 4 (Fig. 6A). However, this technique suffers from the fact that the slope parameter varies over different wavelength ranges (see, for example, the spectrum for the integrated permeate in Fig. 6B). Application of the permeation model to $a_g(\lambda)$ at 23 discrete wavelengths showed a good agreement with the simple reconstruction technique described above, but the slight changes in slope were much better reproduced (e.g., the lower slope between 240 and 280 nm and the steeper slope between 200 and 240 nm; Fig. 6A and B). The contribution of LMW DOM to bulk absorption decreased with increasing wavelengths (Fig. 6A, insert). This is in agreement with the view that small molecules absorb proportionally more at shorter wavelength while larger molecules have more absorption at longer wave-

lengths as indicated by the S_g values. The relatively high LMW contribution at 200–220 nm likely results in part from absorption by nitrate ($\sim 2.3 \text{ m}^{-1}$ per $\mu\text{M NO}_3$ at 200 nm; see Johnson and Coletti, 2002).

The SF spectrum of LMW DOM was reconstructed by application of the permeation model to the fluorescence data measured every 10 nm (Fig. 7A). Over the wavelength range 290–600 nm, each linear regression of $\ln C_p$ vs. $\ln CF$ had an $r^2 > 0.98$. The reconstructed LMW spectrum shows striking similarities with the shape of the integrated permeate spectrum. The fact that such a complex spectrum can be reproduced from the slope and intercept of $\ln FL(\lambda)$ vs. $\ln CF$ is, by itself, a strong demonstration of the applicability and usefulness of the permeation model. Both the integrated

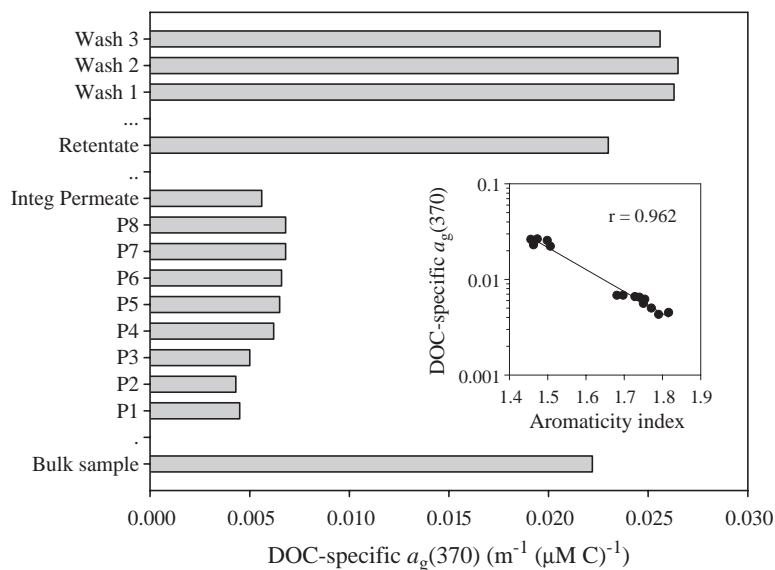


Fig. 4. DOC-specific absorption coefficient at 370 nm, DOC-specific $a_g(370)$. The insert shows the correlation between DOC-specific $a_g(370)$ and the McKnight index of aromaticity ($r=0.962$).

permeate and the reconstructed LMW SF spectra showed a larger peak at 295 nm than the bulk sample (Fig. 7A). This artifact may result from contamination or more likely by the difference in fluorescence quenching linked to differences in pH, ionic strength or metal concentration (Pullin and Cabaniss, 1997; Lu and Jaffe, 2001). Nevertheless, in agreement with data presented by Belzile et al. (2002), practically all the fluorescence peak centered near 295 nm was due to the LMW DOM (Fig. 7B), while the contribution of LMW DOM to SF at longer wavelengths was only 10–36% of bulk sample

fluorescence. This peak centered at 295 nm is generally attributed to the amino acids tryptophan, tyrosine and phenylalanine, to the proteins containing these aromatic amino acids (Yamashita and Tanoue, 2003; Stedmon et al., 2003) or to polyphenol (Scully et al., 2004).

3.4. Comparison with the conventional LMW computation techniques

When the LMW concentrations estimated from the permeation model and permeate time series data are

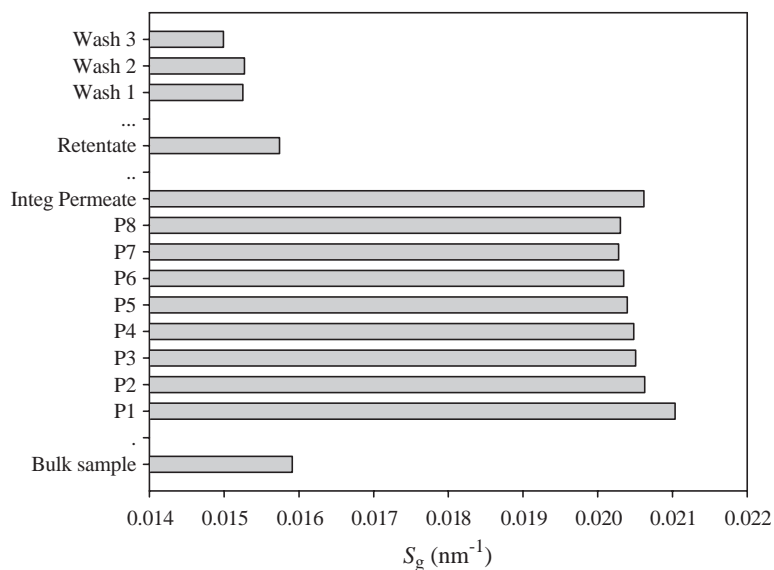


Fig. 5. Slope parameter of the dissolved matter absorption spectra determined over the wavelength range 300–700 nm.

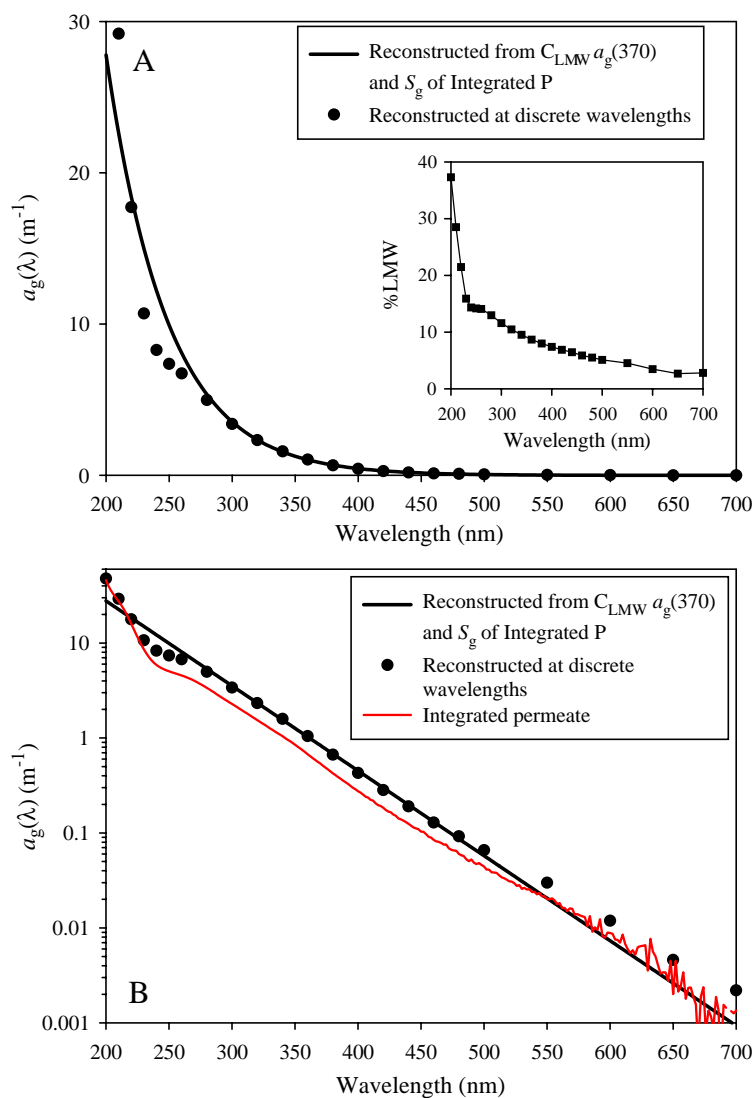


Fig. 6. Reconstructed absorption coefficient spectra $a_g(\lambda)$. In panel (A) the points are the $a_g(\lambda)$ values obtained by applying the permeation model at 23 discrete wavelengths while the line represents the spectrum obtained by applying the permeation model to $a_g(370)$ and using the slope parameter of the integrated permeate to reconstruct the spectrum. In panel (B) the same data are plotted on a ln scale together with the integrated permeate measured spectrum. The insert in panel (A) shows the percent contribution of LMW molecules to bulk absorption.

compared to what would be inferred from measurement of concentrations in the integrated permeate, large discrepancies are observed (Table 3). Using the concentrations measured in the integrated permeate would underestimate the true LMW concentrations by up to 36%. Since the concentrations in the permeate time series samples followed the permeation model, it is straightforward to model the concentrations at higher CF (assuming that the permeation behavior remains constant) and to derive the concentrations that would be measured in the integrated permeate. Fig. 8 shows the modeled and measured concentration in the permeate samples (Fig. 8A and D), in the integrated permeate

(Fig. 8B and E), and the percent contribution of the LMW to bulk concentration and the contribution that would be derived from measurements of the integrated permeate concentration (Fig. 8C and F). For TDN which had a relatively high LMW contribution to bulk concentration (i.e., 65%), the concentration in discrete permeate samples increases only slightly with increasing CF (Fig. 8A), the concentration in the integrated permeate remains fairly constant (Fig. 8B) and the integrated permeate would quickly approach the real LMW concentration (Fig. 8C) with a difference of only 1.5% at CF=10. However, for $a_g(370)$ for which the LMW contribution was very low (8%), the

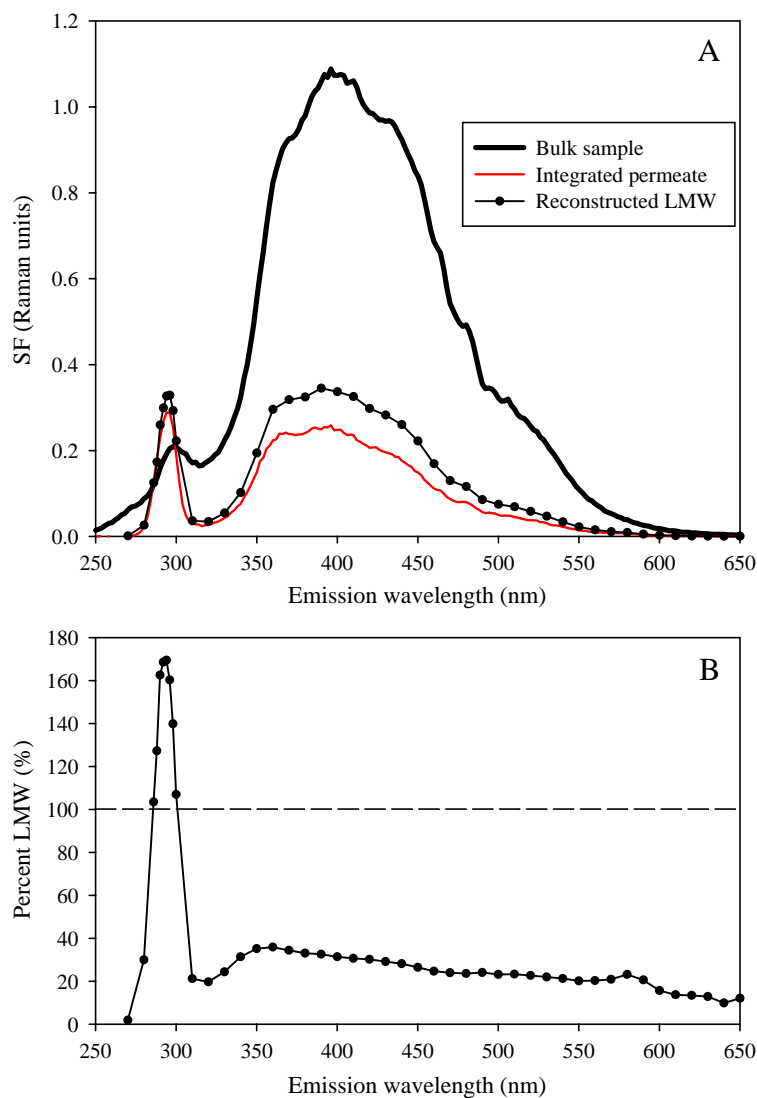


Fig. 7. (A) Synchronous fluorescence (SF) spectrum of LMW DOM reconstructed by application of the permeation model to data measured every 10 nm; for comparison, the bulk sample and integrated permeate spectra are also shown. (B) Percent contribution of LMW DOM to SF in the bulk sample.

concentration in discrete permeate samples strongly increases with CF (Fig. 8D), the concentration in the integrated permeate remains low and would vary over a

factor of 3 (Fig. 8E) and the concentrations in the integrated permeate would remain much lower than the true LMW concentration even at CF=100 (Fig.

Table 3

Comparison of LMW concentrations and optical properties obtained using three different calculation techniques: (1) LMW concentrations calculated using the permeation model (C_{LMW}), (2) LMW concentrations estimated from the integrated permeate (C_{IntegP}), and (3) LMW concentrations calculated as the difference between bulk concentration (C_{bulk}) and colloids concentration (C_{HMW}) calculated from Eq. (6)

	(1) C_{LMW}	(2) C_{IntegP}	Difference %	(3) $C_{bulk}-C_{HMW}$	Difference %
$a_g(370)$ (m^{-1})	0.839	0.540	36	0.794	5
FL(450) (RU)	2.329	1.642	29	2.117	9
SF(250–650) (RU)	0.119	0.088	26	0.108	9
DOC (μM)	119.0	95.7	20	74.6	37
TDN (μM)	14.5	14.0	3	12.9	11

The percent difference relative to C_{LMW} is also presented. Note that the concentrations measured in the 3 washes are included in C_{HMW} .

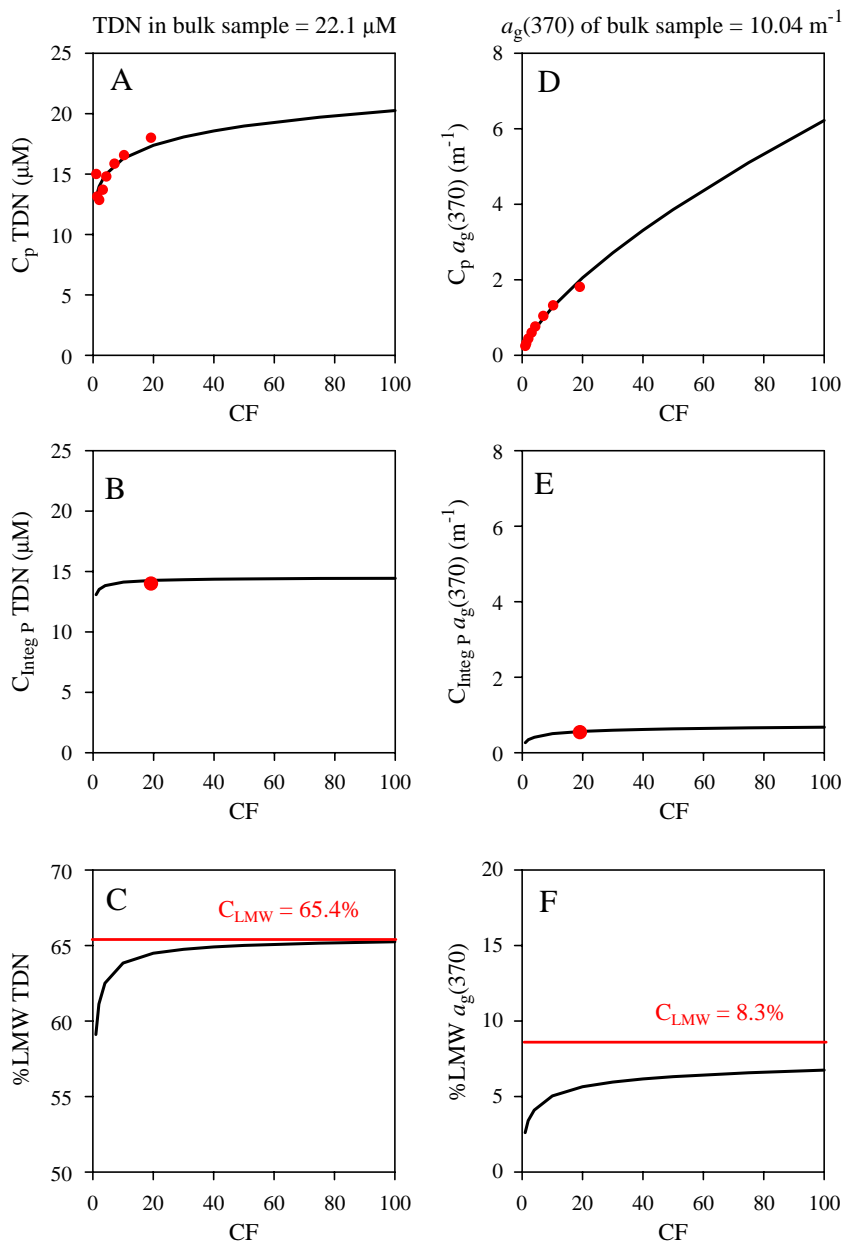


Fig. 8. Modeled (lines) and measured concentration (dots) as of function of the concentration factor. (A–C) Total dissolved nitrogen; and (D–F) dissolved absorption at 370 nm, $a_g(370)$. Permeate samples (A and D), integrated permeate (B and E), and contribution of the LMW to bulk concentration and contribution that would be derived from measurements of the integrated permeate concentration (C and F). C_{LMW} is denoted by a strait line in panels (C) and (F).

8F); at a CF of 4, the LMW contribution would be underestimated by 50%.

In many instances, the results of CFF are interpreted as a function of the retentate concentrations rather than permeate concentration, and the HMW fraction (C_{HMW} or colloidal fraction) is estimated as:

$$C_{\text{HMW}} = (C_{\text{R}} - C_{\text{IntegP}})/\text{CF} \quad (6)$$

where C_{R} and C_{IntegP} refer to the concentrations in the retentate and integrated permeate, respectively (Bueseler et al., 1996). In this case, C_{LMW} is equal to the bulk concentration minus C_{HMW} . As shown in Table 3, at the relatively high CF of 19 used in the present study, this computation technique gave a closer agreement with C_{LMW} for the absorption and fluorescence properties (within 9%), although DOC and TDN concentra-

tions were underestimated by 37 and 11%, respectively. When this computation technique is used, the calculated C_{HMW} and C_{LMW} are strongly dependent on the full recovery of material by cartridge washes.

4. Discussion

The LMW and colloidal DOM fractions isolated from a Yukon River sample using CFF had contrasting optical properties. These markedly different optical properties allowed a new examination of the CFF performance and limitations. Firstly, the absorption and fluorescence spectra, the DOC-specific absorption and the fluorescence quantum yield all indicated the absence of colloids breakthrough the ultrafiltration membrane into the permeate (c.f. Wells, 2002). The increase in permeate absorption, fluorescence and concentrations with increasing CF could be accounted for by the permeation model, and optical spectra reconstructed using this model were coherent with expected shapes and magnitudes. Secondly, the optical properties of the material recovered by three consecutive MilliQ washes were very similar to that of the retentate measured at a CF of 19. This indicates that the material adsorbed to the membrane, if any, was similar in composition to HMW DOM.

When the retentate volume is small compared to the ultrafiltration cartridge volume (like in this study), it is critical to recover all the material contained in the dead volume. Since the results presented here show that the material in the washes had properties typical for the colloidal fraction, the recovery may not be critical for the determination of the LMW fraction from time series permeate data. Nevertheless, it is highly recommended to check for mass balance since different water samples may have different permeation behaviors. Two ways of increasing the proportion of material recovered are (1) to keep the retentate volume large relative to the cartridge volume; and (2) to re-circulate the retentate without applying backpressure for some time at the end of the CFF process so that material associated with the membrane could be displaced by the flow (see Buesseler et al., 1996).

Significant errors in the determination of the contribution of LMW to bulk properties result from the analysis of concentrations in the integrated permeate or retentate obtained at a given CF. The magnitude of this error varies with CF (it is maximum at low CF) but, as our results show, it also varies with the properties considered. At very high CF (e.g., >100), the concentration in the integrated permeate would generally approach the true LMW concentration. However, non-

linear permeation behavior is often observed at high CF, suggesting membrane clogging or concentration-related modifications of the retained DOM (C. Belzile, personal observation). The application of the permeation model to time series samples of permeate therefore appears to be the best way of obtaining quantitative separation of the LMW and colloids fractions from CFF. The results presented here suggest that even for complex, spectral optical properties the permeation model allows reconstruction of the true contributions.

Despite the errors likely introduced by non-optimal use of the CFF technique in previous studies and other limitations mentioned above, we have found variations of the optical properties as a function of DOM molecular weight that are consistent with literature values. When compared to the colloidal fraction, the LMW DOM had a lower aromaticity as indicated by the McKnight index (Fig. 3A), a higher fluorescence quantum yield (Fig. 3B), less absorption per unit DOC (Fig. 4), and an absorption curve with a steeper slope (Fig. 5). All these optical characteristics are consistent with a highly altered LMW DOM pool in the Yukon River contrasting with diagenetically young colloids that are representing >70% of DOM absorption and fluorescence.

5. Conclusions

The only way to avoid variations in the estimation of the LMW and colloidal fractions related to the use of different CFs is to measure the concentration of permeate time series samples and to use the permeation model to reconstruct the LMW and HMW contributions. Ideally, the final CF should be kept low enough to avoid possible concentration-related modifications of the permeation behavior and molecular properties, but high enough for the statistically significant determination of the slope and intercept of the $\ln C_p$ vs. $\ln C_f$ relationships.

The contrasting optical properties of LMW and colloidal DOM indicate that analysis of the optical properties of bulk DOM reveals information regarding its composition and diagenetic state. DOM optics, in conjunction with molecular-level chemical characterization, is a valuable tool that will help understand the biogeochemical cycling of this globally important pool of organic matter.

We have found more than 67% of DOC and DOM color and fluorescence in the Yukon River near its discharge into the Bering Sea to be colloidal, and therefore highly reactive and potentially labile. This observation, coupled with the relatively high DOC

concentration measured and the large river discharge, points to the importance of the Yukon River as a source of reactive DOM to the Bering Sea. This highly colored colloidal DOM may be subject to photodegradation in the coastal ocean, simultaneously causing its direct mineralization and increasing its availability to bacteria. These two pathways lead to the release of greenhouse gases to the atmosphere, with possible interaction with global climate change.

Acknowledgements

We thank Chunhao Xu, Joe Prince and Lloyd Heckman for field assistance. This work was funded by NSF (EAR#0403596) and the International Arctic Research Center, University of Alaska Fairbanks. Comments from two anonymous reviewers improved the manuscript.

References

- Amon, R.M.W., Benner, R., 1996. Bacterial utilization of different size classes of dissolved organic matter. *Limnol. Oceanogr.* 41, 41–51.
- Belzile, C., Gibson, J.A.E., Vincent, W.F., 2002. CDOM and DOC exclusion from lake ice: implications for irradiance transmission and carbon cycling. *Limnol. Oceanogr.* 47, 1283–1293.
- Brabets, T.P., 2003. Fixed-station samples. In: Schuster, P.F. (Ed.), *Water and Sediment Quality in the Yukon River Basin, Alaska, During Water Year 2001, Open-File Report* (United States Geological Survey), vols. 03–427, pp. 3–22.
- Buesseler, K.O., Bauer, J.E., Chen, R.F., Eglinton, T.I., Gustafsson, O., Landing, W., Mopper, K., Moran, S.B., Santschi, P.H., VernonClark, R., Wells, M.L., 1996. An intercomparison of cross-flow filtration techniques used for sampling marine colloids: overview and organic carbon results. *Mar. Chem.* 55, 1–31.
- Chin, Y.-P., Aiken, G., O'Loughlin, E., 1994. Molecular weight, polydispersity, and spectroscopic properties of aquatic humic substances. *Environ. Sci. Technol.* 28, 1853–1858.
- Chin, W.-C., Orellana, M.V., Verdugo, P., 1998. Spontaneous assembly of marine dissolved organic matter into polymer gels. *Nature* 391, 568–572.
- Guo, L., Santschi, P.H., 1996. A critical evaluation of the cross-flow ultrafiltration technique for sampling colloidal organic carbon in seawater. *Mar. Chem.* 55, 113–127.
- Guo, L., Wen, L.-S., Tang, D., Santschi, P.H., 2000. Re-examination of cross-flow ultrafiltration for sampling aquatic colloids: evidence from molecular probes. *Mar. Chem.* 69, 75–90.
- Guo, L., Hunt, B.J., Santschi, P.H., 2001. Ultrafiltration behavior of major ions (Na, Ca, Mg, F, Cl, and SO₄) in natural waters. *Water Res.* 35, 1500–1508.
- Hama, T., Yanagi, K., Hama, J., 2004. Decrease in molecular weight of photosynthetic products of marine phytoplankton during early diagenesis. *Limnol. Oceanogr.* 49, 471–481.
- Johnson, K.S., Coletti, L., 2002. In situ ultraviolet spectrophotometry for high resolution and long-term monitoring of nitrate, bromide and bisulfide in the ocean. *Deep-Sea Res.* 1 49, 1291–1305.
- Logan, B.E., Jiang, Q., 1990. Molecular size distributions of dissolved organic matter. *J. Environ. Eng.* 116, 1046–1062.
- Lu, X., Jaffe, R., 2001. Interaction between Hg(II) and natural dissolved organic matter: a fluorescence spectroscopy based study. *Water Res.* 35, 1793–1803.
- Markager, S., Vincent, W.F., 2000. Spectral light attenuation and the absorption of UV and blue light in natural waters. *Limnol. Oceanogr.* 45, 642–650.
- McKnight, D.M., Boyer, E.W., Westerhoff, P.K., Doran, P.T., Kulbe, T., Andersen, D.T., 2001. Spectrofluorometric characterization of dissolved organic matter for indication of precursor organic material and aromaticity. *Limnol. Oceanogr.* 46, 38–48.
- Moran, M.A., Zepp, R.G., 1997. Role of photoreactions in the formation of biologically labile compounds from dissolved matter. *Limnol. Oceanogr.* 42, 1307–1316.
- Ohno, T., 2002. Fluorescence inner-filtering correction for determining the humification index of dissolved organic matter. *Environ. Sci. Technol.* 36, 742–746.
- Pullin, M.J., Cabaniss, S.E., 1997. Physicochemical variations in DOM-synchronous fluorescence: implications for mixing studies. *Limnol. Oceanogr.* 42, 1766–1773.
- Scully, N.M., Maie, N., Dailey, S.K., Boyer, J.N., Jones, R.D., Jaffe, R., 2004. Early diagenesis of plant-derived dissolved organic matter along a wetland, mangrove, estuary ecotone. *Limnol. Oceanogr.* 49, 1667–1678.
- Stedmon, C.S., Markager, S., Bro, R., 2003. Tracing dissolved organic matter in aquatic environments using a new approach to fluorescence spectroscopy. *Mar. Chem.* 82, 239–254.
- Stewart, A.J., Wetzel, R.G., 1980. Fluorescence: absorbance ratio—a molecular-weight tracer of dissolved organic matter. *Limnol. Oceanogr.* 25, 559–564.
- Traina, S.J., Novak, J., Smeck, N.E., 1990. An ultraviolet absorbance method of estimating the percent aromatic carbon content of humic acids. *J. Environ. Qual.* 19, 151–153.
- Twardowski, M.S., Boss, E., Sullivan, J.M., Donaghay, P.L., 2004. Modeling the spectral shape of absorption by chromophoric dissolved organic matter. *Mar. Chem.* 89, 68–88.
- Vaillancourt, R.D., Balch, W.M., 2000. Size distribution of marine submicron particles determined by flow field-flow fractionation. *Limnol. Oceanogr.* 45, 485–492.
- Wells, M.L., 2002. Marine colloids and trace metals. In: Hansell, D.A., Carlson, C.A. (Eds.), *Biogeochemistry of Marine Dissolved Organic Matter*. Elsevier, pp. 367–404.
- Yacobi, Y.Z., Alberts, J.J., Takács, M., McElvaine, M., 2003. Absorption spectroscopy of colored dissolved organic carbon in Georgia (USA) rivers: the impact of molecular size distribution. *J. Limnol.* 62, 41–46.
- Yamashita, Y., Tanoue, E., 2003. Chemical characterization of protein-like fluorophores in DOM in relation to aromatic amino acids. *Mar. Chem.* 82, 255–271.